

# INTEGRATED MICRO X-RAY FLUORESCENCE AND CHEMOMETRIC ANALYSIS FOR PRINTED CIRCUIT BOARDS RECYCLING

Silvia Serranti \*, Giuseppe Capobianco and Giuseppe Bonifazi

DICMA, Department of Chemical Engineering, Materials and Environment, Sapienza - University of Rome, via Eudossiana 18, 00184 Rome, Italy

## Article Info:

Received:  
15 January 2018  
Revised:  
01 March 2018  
Accepted:  
19 March 2018  
Available online:  
31 March 2018

## Keywords:

WEEE  
X-ray fluorescence  
Printed circuit boards  
Characterization  
Recycling

## ABSTRACT

A novel approach, based on micro X-ray fluorescence ( $\mu$ XRF), was developed to define an efficient and fast automatic recognition procedure finalized to detect and topologically assess the presence of the different elements in waste electrical and electronic equipment (WEEE). More specifically, selected end-of-life (EOL) iPhone printed circuit boards (PCB) were investigated, whose technological improvement during time, can dramatically influence the recycling strategies (i.e. presence of different electronic components, in terms of size, shape, disposition and related elemental content). The implemented  $\mu$ XRF-based techniques allow to preliminary set up simple and fast quality control strategies based on the full recognition and characterization of precious and rare earth elements as detected inside the electronic boards. Furthermore, the proposed approach allows to identify the presence and the physical-chemical attributes of the other materials (i.e. mainly polymers), influencing the further physical-mechanical processing steps addressed to realize a pre-concentration of the valuable elements inside the PCB milled fractions, before the final chemical recovery.

## 1. INTRODUCTION

PCB are an essential part of all technological devices commonly utilized by consumers. The development of technology and society, as well as the higher performance of the electronic devices, and the corresponding miniaturization, produce, as a consequence, an increase of the waste electrical and electronic equipment (WEEE) to be disposed of (Zhou et al., 2010). Precious and rare earth elements are around us, not only in nature but in our everyday lives (i.e. car, computer, smartphone, energy-efficient fluorescent lamp, and color TV, as well as in lasers, lenses, ceramics and in many other products). We need rare earths for so many applications, but their supply is restricted to few mining districts in the world, this fact led these elements to create a critical-metals agenda. (Chakhmouradian et al., 2012). To face this crucial situation, the European Commission in 2008, through the "European Raw Materials Initiative" (European Commission, 2008) suggested a combined strategy based on enforcing deeper links and co-operation contracts with producer countries (by improving foreign investment agreements), encouraging and promoting internal mining potential and developing more efficient recycling policies (Massari et al., 2013; Tiess et al., 2010). An ad-hoc working group of the European Union

has determined a set of critical resources as: Be, Co, Ga, Ge, In, Mg, Nb, Ta and W, the platinum group metals (PGM): Pt, Pd, Rh, Ru, Os, Ir) and rare earth elements (REE) (European Commission, 2010). Starting from these premises the possibility to utilize specific EOL products as secondary raw materials sources, the recovery of precious and rare earth elements, practically "became a must". The concept of "urban mining", referred to the different EOL materials and/or manufactured products of human origin, was thus introduced: precious and rare earth elements in dismissed electronic units of large use as mobile phones, "tablets" and personal computers, thus representing an important secondary raw materials source (Hagelüken et al., 2010; Palmieri et al., 2014).

The most commonly applied techniques for determination of rare earth elements are inductively coupled plasma-optical emission spectrometry (ICP-OES), inductively coupled plasma mass spectrometry (ICP-MS), X-ray fluorescence (XRF) and neutron activation analysis (NAA) (Zawisza et al., 2011). ICP-MS and ICP-OES require a preliminary strong manipulation of the samples in order to separate the rare earth element from the matrix. This approach is complex, time-consuming, and can always be a potential source of random, or even systematic, errors. The NAA technique has been increasingly utilized to de-

\* Corresponding author:  
Silvia Serranti  
email: [silvia.serranti@uniroma1.it](mailto:silvia.serranti@uniroma1.it)



tect the presence of rare earth elements in solid samples. Sometimes, NAA presents practical implementation problems mainly due to interference and the required long radiation time (Kumar et al., 2014). Recently also laser-induced breakdown spectroscopy (LIBS) techniques (Carvalho et al., 2015) have been successfully applied to determine rare earth elements. The XRF technique offers the possibility to determine rare earth elements in solid materials not requiring, as for LIBS, any specific sample preparation; it also allows simultaneous determination of both trace and main components (Zhang et al., 2007; De Vito et al., 2007; Smoliński et al., 2016). However, to obtain a correct quantification of the detected elements it is necessary to consider matrix effects (absorption and enhancement) and peaks overlapping. Theoretically, the intensity of a peak is linearly proportional to the concentration of the analyte, but practically the intensity of a peak does not depend only on the concentration of the respective elements, but it is also determined by presence and concentrations of other elements and by the interaction with matrix (Smoliński et al., 2016).

The new generation of scanning XRF analytical units, based on confocal XRF method, realizes the best acquisition conditions, both in terms of speed and analytical data set reliability. For every acquired hyper-map, a XRF spectrum is associated to each pixel. Thus, an acquisition consists in a  $n \times m$  matrix of spectra, where  $n$  and  $m$  are the number of pixels in the  $x$  and  $y$  direction, respectively. Analyzing every spectrum associated to each pixel, it is possible to know the total counts corresponding to a given energy. By selecting the energy ranges depicted in the spectrum, it is possible to obtain a 2D image corresponding to the distribution of selected elements (Figueroa et al., 2014).

Aim of this work is to verify the possibility to utilize the confocal  $\mu$ XRF imaging based approach as an analytical technique to perform an automatic detection and mapping of the elements present in dismissed iPhone PCB and/or in the products (i.e. particles) resulting from their mechanical-physical processing before the final chemical recovery (i.e. leaching). Following this approach, it is thus not necessary the presence of an operator performing a preliminary identification/selection of the different energy ranges/peaks representative of a specific element. To reach this goal, data were analyzed by chemometric techniques (exploration and classification methods) and the results compared with the maps of the elements obtainable by the classical approach, that is the manual selection of the energy ranges associated to each pixel. This approach could be successfully applied to perform quality control actions referred to other WEEE and resulting milled/classified products for precious and rare earth elements chemical recovery.

## 2. MATERIALS AND METHODS

### 2.1 Samples and experimental set up

The reference PCB samples utilized for the analysis are constituted by 3 electronic boards belonging to 3 different iPhone models (i.e. iPhone 4, iPhone 3s and iPhone 4s)

(Figure 1). Investigations have been carried out with reference to 8 elements (palladium, silver, gold, zinc, copper, tantalum, lead and iron), being among those of higher interest in terms of recovery and/or interfering actions, when XRF analyses are performed.

Precious and rare earth elements are in a small concentration on each electronic board, however the preliminary correct identification, and further separation, when applied on large quantities, allow the process to be economically valid (Bonifazi et al., 2017).

The  $\mu$ XRF based elements mapping was performed at Raw-Ma Lab (Raw materials Laboratory) of the Department of Chemical Engineering, Materials & Environment (Sapienza - University of Rome, Italy) using a benchtop spectrometer (M4 Tornado, Bruker®) equipped with a Rh X-ray tube with poly-capillary optics as the X-ray convergence technique, and XFlash® detector providing an energy resolution better than 145 eV and 5 filters (Guerra et al., 2013).

The whole spectra comprised 4096 channels with a spot size of approximately 30  $\mu$ m. Spectrum energy calibration was daily performed before each analysis batch by using zirconium (Zr) metal (Bruker® calibration standard). The sensitivity of  $\mu$ XRF is determined by the excitation probability of the sample and the peak to background ratio. The background intensities were directly computed by the equipment (ESPRIT Bruker® software). The sample chamber can be evacuated to 20 mbar and, therefore, light elements such as sodium can be measured (Nikonow et al., 2016). Constant exciting energies of 50 kV and 500  $\mu$ A, were adopted for acquisition. The set up mapping acquisition parameters were a pixel size of 80  $\mu$ m and an acquisition time, for each pixel, of 6 milliseconds. Spectral data (i.e. hyper-maps) analysis was carried out adopting chemometric methods, using the PLS\_Toolbox (version 8.2.1, Eigenvector Research, Inc.) running inside MATLAB (version 9.1.0, The Mathworks, Inc.).

### 2.2 $\mu$ XRF: acquisition and data handling

The experimental procedure was defined and implemented in two steps: the 1st one finalized to the acquisi-

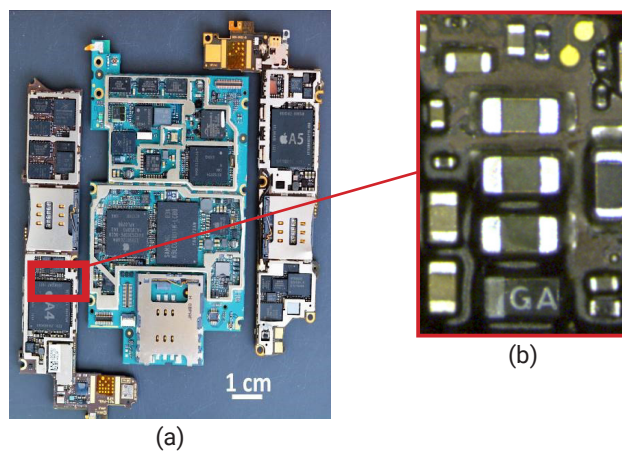


**FIGURE 1:** Digital image representing the electronic 3 acquired boards (a) and an example of one of the region of interest (ROI) selected to set up the best filtering/acquisition conditions (b).

tion of the hyper-maps and the further XRF peaks deconvolution and the 2nd one addressed to the acquisition of the calibration standards and to the classification of the different elements detected in the electronic boards.

### 2.2.1 Step 1: hyper-maps acquisition and XRF peak deconvolution

Smartphone electronics boards (Figure 1a) were acquired by  $\mu$ XRF in order to build hyper-maps of all the elements. Small regions of interest (ROI) (Figure 1b) of the electronics boards were selected and acquired utilizing different filters in order to set up the best conditions to reduce the signal of light elements (i.e. silicon) maximizing, at the same time, the signal of precious and rare earth elements (Gallardo et al., 2016). One of the main strategies to apply in order to improve measurement conditions for elements of interest is, in fact, the utilization of primary beam filters, aluminum made, that are placed between the X-ray source and the sample. In the Bruker M4 Tornado  $\mu$ XRF device, five internal filters are available (Al 12.5  $\mu$ m, Al 100  $\mu$ m, Al 630  $\mu$ m, Al/Ti 100/25  $\mu$ m and Al/Ti/Cu 100/50/25  $\mu$ m).

### 2.2.2 Step 2: acquisition of calibration standards and identification of elements by Partial Least Squared Discriminant Analysis (PLS-DA)

Calibration standard were acquired by  $\mu$ XRF to build a classification model able to recognize the different elements without any human based investigation finalized to optimal mapping set up to enhance the presence of precious metals and rare earths. A set of 8 elements clearly identified in the dataset as palladium, silver, gold, zinc, copper, tantalum, lead and iron was used as training dataset to build the classification model (Figure 2). The classification model was then validated utilizing the electronic boards dataset generated by the experimental approach described

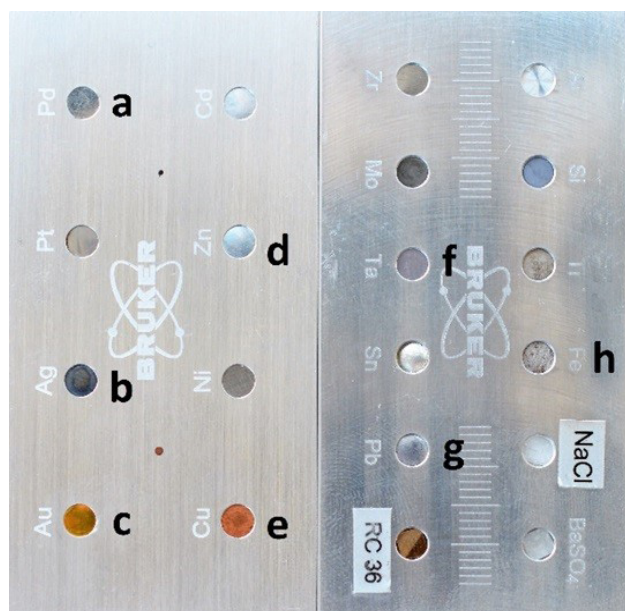


**FIGURE 2:** Digital image representing the acquired standard calibration elements: a: palladium, b: silver, c: gold, d: zinc, e: copper, f: tantalum, g: lead and h: iron.

in Step 1.

Spectral data analysis was preliminary addressed to explore and to evaluate the quality of the acquired information to be utilized for the further classification model definition, design, implementation and set up. To reach these goals, a preliminary *Principal Component Analysis* (PCA) and a further *Partial Least Squares Discriminant Analysis* (PLS-DA) were carried out.

PCA is the most utilized multivariate data analysis method for exploratory data handling, outlier detection, rank (dimensionality) reduction, graphical clustering, classification, regression, etc. (Bro et al., 2014). It was used to decompose the “pre-processed” spectral data into several principal components (PCs) (linear combinations of the original spectral data) embedding the spectral variations of each collected spectral data set. According to this approach, a reduced set of factors is produced and used for discrimination since it provides an accurate description of the entire dataset. The first few PCs, resulting from PCA, are generally utilized to analyze the common features among samples and their grouping: samples characterized by similar spectral signatures tend to aggregate in the score plot of the first two or three components. Spectra could be thus characterized either by the reflectance at each wavenumber in the wavenumber space, or by their score on each PC in the PC space (Bro et al., 2014). Samples characterized by similar spectra, belonging to the same class of products, are grouped in the same region of the score plot related to the first two or three PCs, whereas samples characterized by different spectral features will be clustered in other parts of this space.

PLS-DA was used to find a model able to perform an optimal discrimination among classes of samples and to predict new images. PLS-DA is a supervised classification technique, requiring a prior knowledge of the data (Ballabio et al., 2013). PLS-DA is used to classify samples into pre-defined groups by forming discriminant functions from input variables (KeV) to yield a new set of transformed values providing a more accurate discrimination than any single variable. A discriminant function is then built using samples with known groups to be employed later to classify samples with unknown group set. Therefore, once the model is obtained, it can be applied to an entire hypercube and for the classification of new hypercubes. The result of PLS-DA, applied to the hyperspectral images, is a “prediction map,” where the class of each pixel can be identified using color mapping.

## 3. RESULTS AND DISCUSSION

Results and discussion are reported in the following, presenting and comparing the classical human based  $\mu$ XRF mapping approach and the proposed one based on PLS-DA classification.

### 3.1 Step 1: acquisition of hypermaps and deconvolution of XRF peaks

The “preliminary” hyper-maps acquisition of the selected ROIs was carried out adopting two different aluminum filters (Al100 and Al630), whose aim is mainly to reduce

the signal due to Si and Ba presence, thus allowing better heavy metals display, and the results were compared with those obtained with the acquisition without filter. An example is reported in Figure 3. The map of the elements, referred to the ROI, clearly shows as the detection of gold and of the other heavy elements is negatively affected by the presence of silicon and barium, present on electronic board surface.

The same ROI acquired with the Al100 filter shows a better “visualization” of gold and other heavy elements. The “noise effect” related to silicon and barium is reduced. Finally, the acquisition with Al630 filter shows the same gold distribution as that obtained using the Al100 filter, producing a stronger reduction of the signal associated to all the lighter elements (i.e. lower atomic number than barium). It was thus chosen to perform the acquisition of the hyper-maps, for all the boards, utilizing the Al100 filter. Following this strategy it was thus possible to obtain a better detection of precious and rare earth elements, reducing, at the same time, the negative effects of the signal of all those elements not of interest for this study, as silicon (Figure 4).

### 3.2 Step 2: Acquisition of calibration standards and identification of elements by PLS-DA

Calibration standards were acquired adopting the same experimental conditions utilized to perform the electronic boards hyper-mapping (Figure 5). Starting from the acquired raw data of the different calibration elements, currently utilized as standards (i.e. palladium, silver, gold, zinc, copper, tantalum, lead and iron), reference energy spectra have been selected.

The reference energy spectra associated to each element show different signatures (Figure 6a). Each energy spectra is characterized by several peaks according to the emission of a photon quantum (fluorescence radiation), related to the energy difference between the inner and outer shell. To emphasize the spectral characteristics of all the elements, “only” the mean spectra between 0 and 20 KeV, have been considered, processed and mean centered (Figure 6b), before the application of PCA. The PCA score plot allows identifying eight distinct groups according their spectral signature.

The 3D score plot (PC1-PC4-PC6) reported in Figure 7a shows a good separation (i.e. distinction) of all the el-

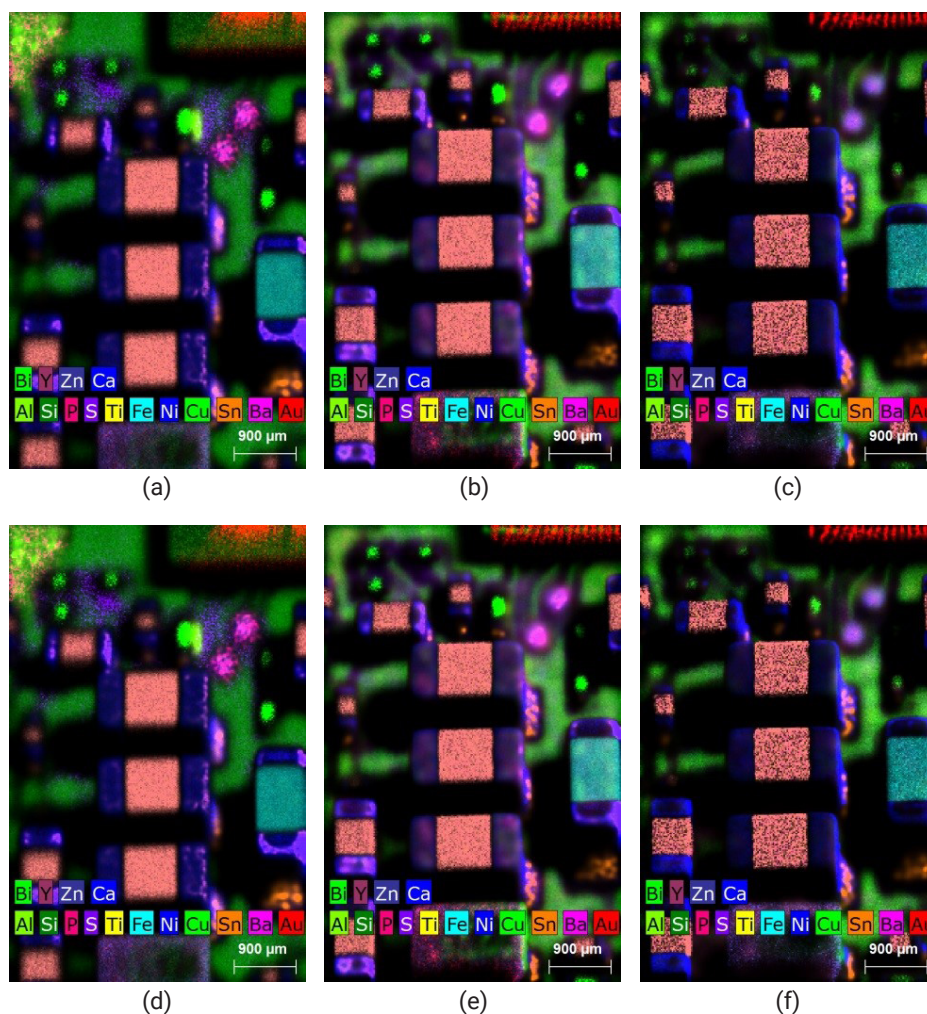


**FIGURE 3:** Hyper-maps of the elements detected by  $\mu$ XRF without filtering (a) and utilizing a Al100 (b) and a Al630 (c) filters, respectively. Detail of the distribution of gold and silicon without filtering (d) and utilizing a Al100 (e) and a Al630 (f) filters.



(a)

**FIGURE 4:** Hyper-map of all elements detected by  $\mu$ XRF (a) and associated average concentration of the different elements as detected by acquisition (b).

Element	Series	[Norm.wt. %]
Silicon	<i>K-series</i>	49.56
Copper	<i>K-series</i>	21.42
Nickel	<i>K-series</i>	7.71
Iron	<i>K-series</i>	6.60
Zinc	<i>K-series</i>	3.09
Chromium	<i>K-series</i>	2.90
Barium	<i>L-series</i>	2.86
Tin	<i>L-series</i>	2.56
Calcium	<i>K-series</i>	0.92
Titanium	<i>K-series</i>	0.77
Tantalum	<i>L-series</i>	0.38
Palladium	<i>K-series</i>	0.33
Silver	<i>K-series</i>	0.27
Gold	<i>L-series</i>	0.27
Strontium	<i>K-series</i>	0.14
Aluminium	<i>K-series</i>	0.14
Yttrium	<i>K-series</i>	0.04
Lead	<i>L-series</i>	0.03
Bismuth	<i>L-series</i>	0.02
Sum:		100

(b)

elements, as well as a high uniformity for each class. The loadings of PC1, PC4 and PC6 (Figure 7b) show, in the region between 3 KeV and 15 KeV, the high variance of data, as a consequence 7 principal components are necessary to explain the variation of the calibration.

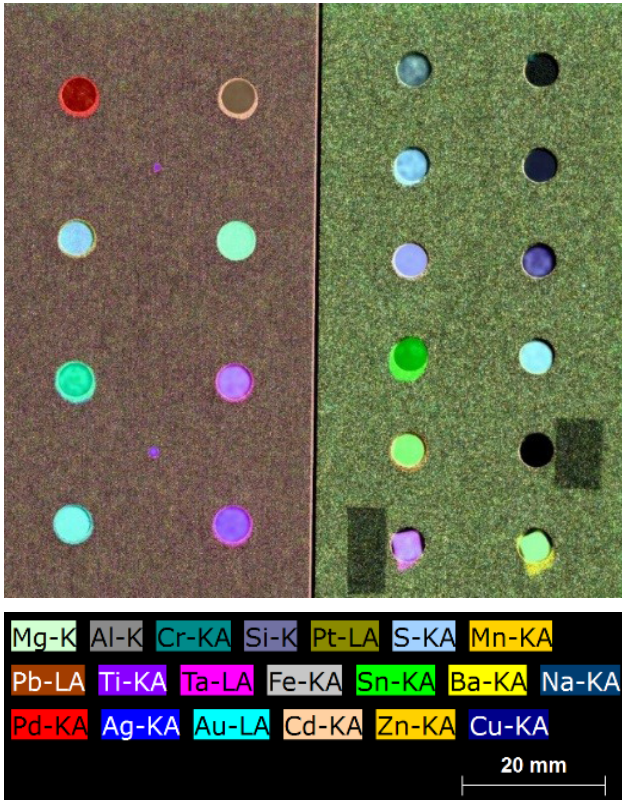


**FIGURE 5:** Elements hyper-maps of the calibration standards.

The selected energy spectra have been thus adopted as training dataset and a PLS-DA model was built. The obtained values of Sensitivity and Specificity are shown in Table 1.

The Sensitivity estimates the model ability to avoid false negatives (i.e. number of samples of a given type correctly classified as that type).

The Specificity estimates the model ability to avoid false positives (the number of samples not of a given type correctly classified as not of that type).

Sensitivity and Specificity can be assumed as model efficiency indicators: the more the values are close to one, the better the modelling is. In this study, the obtained values for Sensitivity and Specificity are very good. To verify its classification ability, the built PLS-DA model was applied to the electronic boards data set.

The results in terms of prediction (i.e. "Pred Probability") are shown in Figures 8-15: the class with the highest probability to belong to the chemical element, object of the detection/recognition, is assigned to each pixel in the image. The obtained results are very good for all the investigated elements, being comparable with those obtained following the classical "instrument-men-driven" approach. Misclassifications sometimes occur, but they are mainly due to the border effect or to the co-existence of several elements in the same pixel.

The element map of palladium (Pd) shows a low concentration but a wide distribution with a greater presence on micro-processors and electronic components according to their large utilization in electronic industry (Figure 8a). The prediction shows in the same area, mapped by  $\mu$ XRF, the presence of palladium confirming the good quality of the PLS-DA based modelling (Figure 8b).

The element map of gold (Au) shows a greater concen-

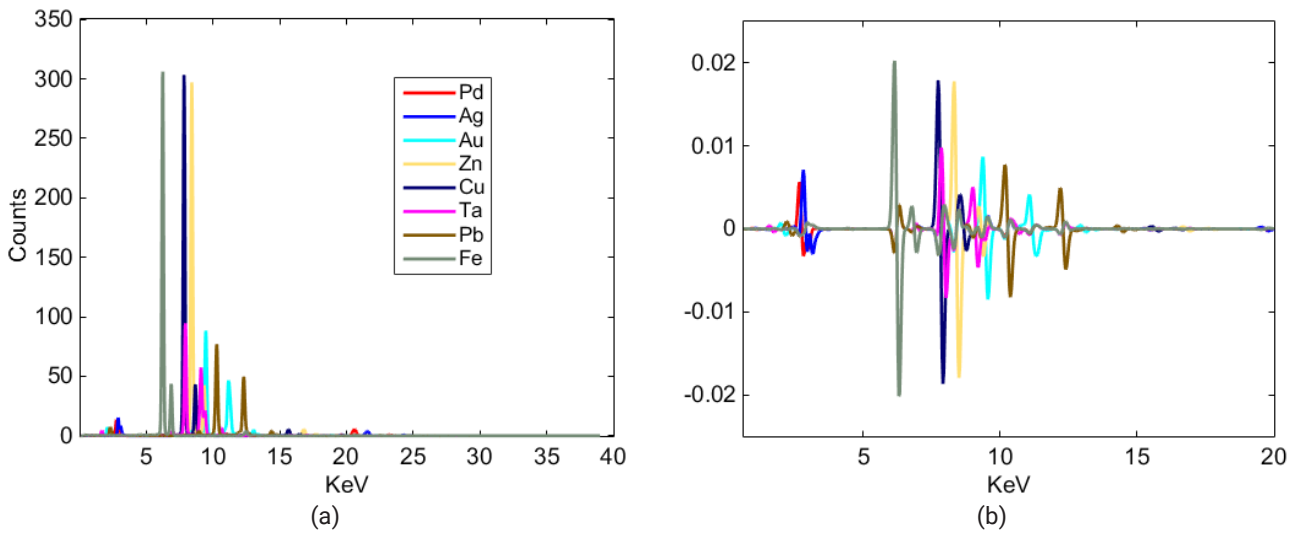


**FIGURE 6:** Raw (a) and pre-processed spectra (b), as resulting from the sequential application of the functions: Normalize (1-Norm, Area = 1), Baseline, Smoothing (order: 0, window: 5 pt, incl only, tails: polyinterp), 1st Derivative (order: 2, window: 7 pt, incl only, tails: polyinterp) and Mean Center.

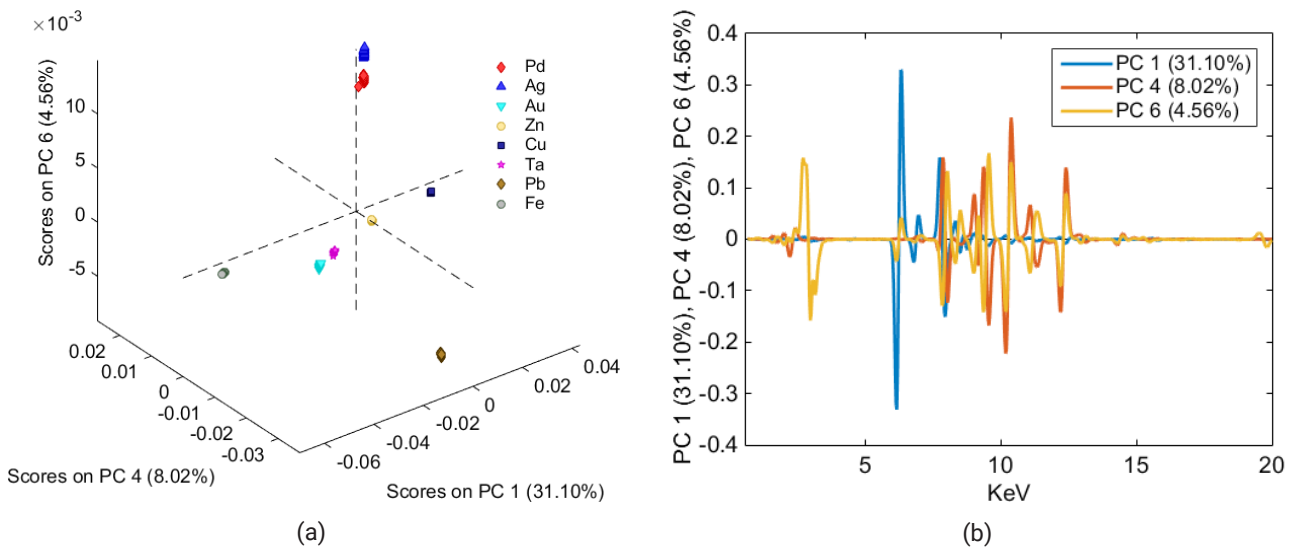


**FIGURE 7:** 3D PCA score plot (PC1-PC4-PC6) referred to the different investigated elements (a) and corresponding plot of the loadings (b).

tration of this element both with reference to component connector regions and also inside some components. In this latter case, detection is commonly realized when higher energies are utilized. The inner detection is also affected by the materials embedding gold elements (Figure 9a). The prediction map shows in the same area, mapped by  $\mu$ XRF, the presence of gold with a low error in classification related to its large presence (Figure 9b).

Silver (Ag) mapping shows a low concentration of this element, but a large distribution on electronic boards, as a consequence the signal is difficult to separate from background and border effects are significant (Figure 10a). The prediction map of silver shows the same characteristics, as detected by classical  $\mu$ XRF analysis. Silver topological assessment on the board is difficult to quantify, however, some electronic components show, in prediction, greater concentration (Figure 10b), if compared with the classical  $\mu$ XRF analysis.

The element map of zinc (Zn) clearly allows to identify the presence of this element both in the electronic components and in the protection structures (Figure 11a). The prediction maps show the presence of zinc in the same areas confirming the good discrimination and prediction power of the PLS-DA model (Figure 11b).

The element map of copper (Cu) shows a large concentration and distribution according to the high use of this material inside the electronic component (i.e. printed circuit tracks) (Figure 12a) The prediction maps show the same large distribution of copper to its topological assessment as resulting from classical  $\mu$ XRF maps (Figure 12b).

The element map of tantalum (Ta) shows its presence only in some electronic component. The total concentration of tantalum on electronic board is very low. Its primary peak (La=8.146 KeV) overlaps copper peak (Ka=8.046 KeV), therefore to perform tantalum mapping the secondary peak (Lb=9.343 KeV) was selected because it is not in-

**TABLE 1:** Sensitivity and Specificity for the PLS-DA built model.

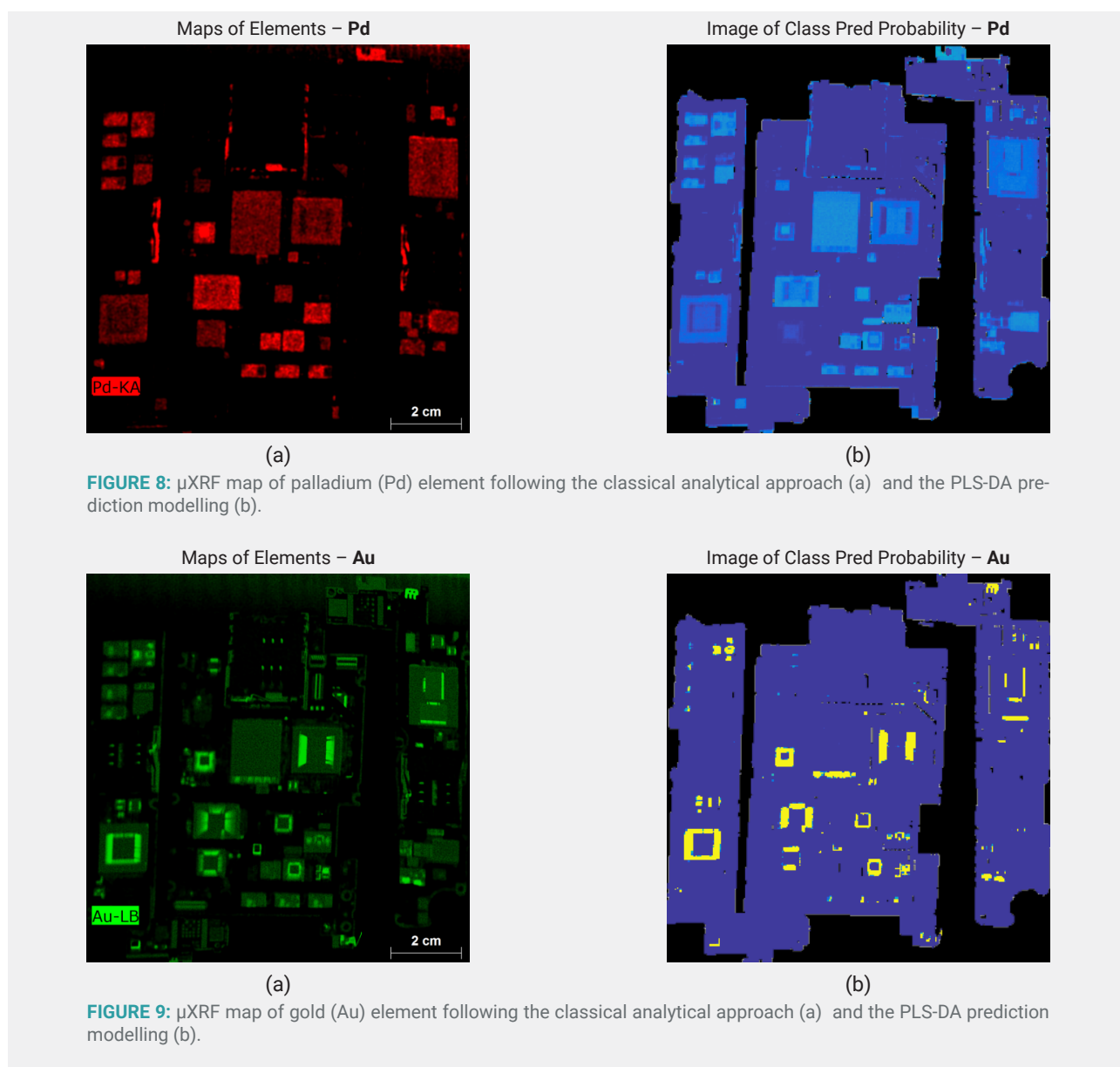
Modeled Class: 1	Pd	Ag	Au	Zn	Cu	Ta	Pb	Fe
Sensitivity (Cal):	1.000	1.000	1.000	1.000	1.000	1.000	1.000	1.000
Specificity (Cal):	1.000	0,984	1.000	1.000	1.000	1.000	1.000	1.000
Sensitivity (CV):	1.000	1.000	1.000	1.000	1.000	1.000	1.000	1.000
Specificity (CV):	0.990	0.997	1.000	1.000	1.000	1.000	1.000	0.997
Class. Err (Cal):	0	0.008	0	0	0	0	0	0
Class. Err (CV):	0.005	0.002	0.012	0	0	0	0	0.161

*Cal: Calibration - CV: Cross validation*

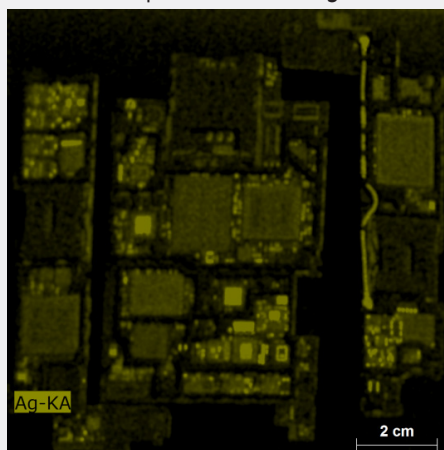
fluenced by the presence, around the same KeV, of peaks representative of other elements (Figure 8a). The prediction of tantalum shows a correct identification according to classical element mapping results. Only in one electronic component its presence was not predicted by modelling, the reason is probably related of the high presence of oth-

er elements (i.e. zinc, gold), generating a different spectral shape compared to the reference one obtained by the tantalum reference calibration dataset (Figure 8b).

The element map of lead (Pb) shows its presence in some circuit components. The total concentration of lead results very low (Figure 14a). The lead prediction map

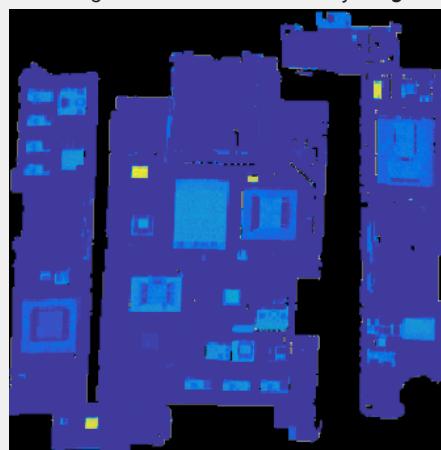


Maps of Elements – Ag



(a)

Image of Class Pred Probability – Ag



(b)

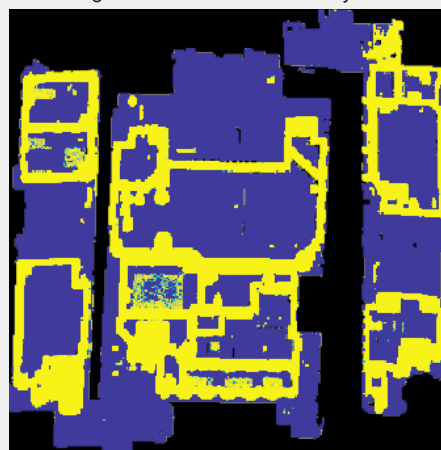
**FIGURE 10:**  $\mu$ XRF map of silver (Ag) element following the classical analytical approach (a) and the PLS-DA prediction modelling (b).

Maps of Elements – Zn



(a)

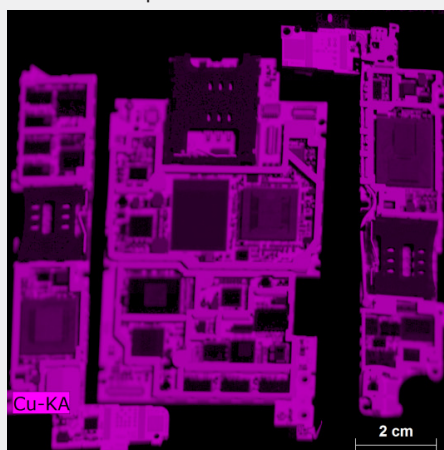
Image of Class Pred Probability – Zn



(b)

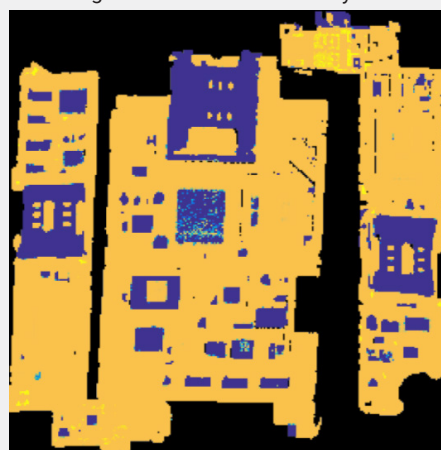
**FIGURE 11:**  $\mu$ XRF map of zinc (Zn) element following the classical analytical approach (a) and the PLS-DA prediction modelling (b).

Maps of Elements – Cu



(a)

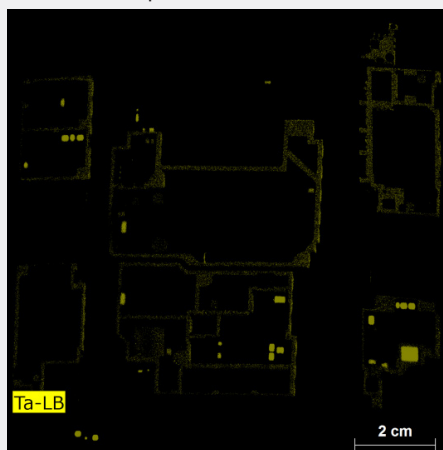
Image of Class Pred Probability – Cu



(b)

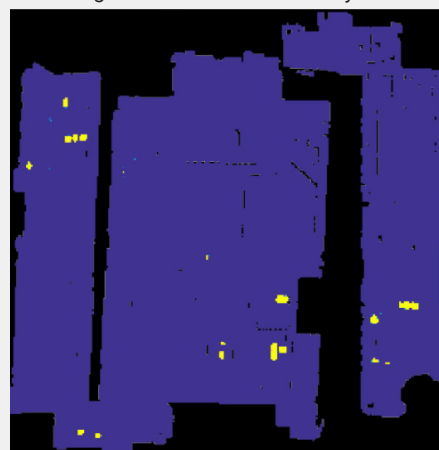
**FIGURE 12:**  $\mu$ XRF map of copper (Cu) element (a) following the classical analytical approach and as resulting from the PLS-DA prediction

Maps of Elements – Ta



(a)

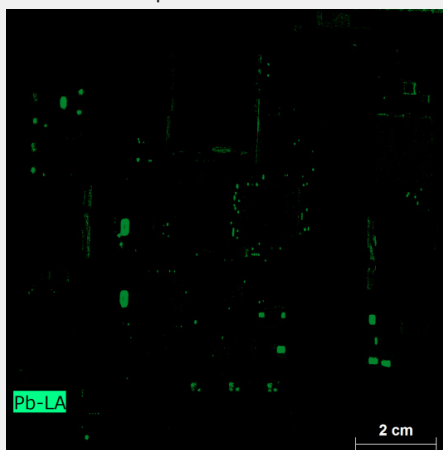
Image of Class Pred Probability – Ta



(b)

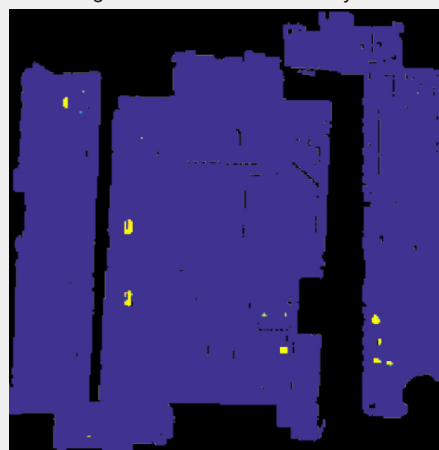
**FIGURE 13:**  $\mu$ XRF map of tantalum (Ta) element following the classical analytical approach (a) and the PLS-DA prediction modelling (b).

Maps of Elements – Pb



(a)

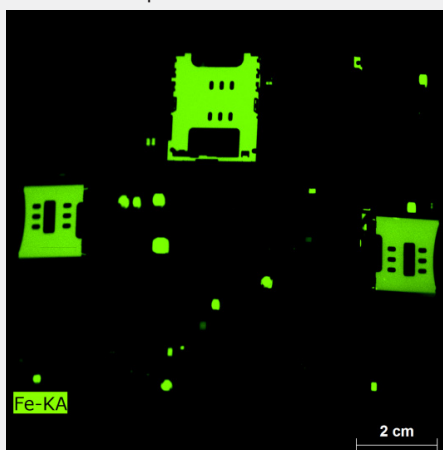
Image of Class Pred Probability – Pb



(b)

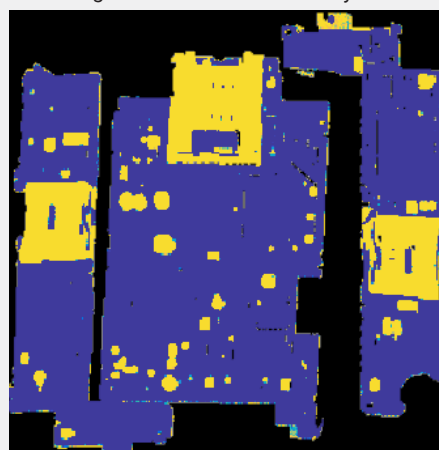
**FIGURE 14:**  $\mu$ XRF map of lead (Pb) element following the classical analytical approach (a) and the PLS-DA prediction modelling (b).

Maps of Elements – Fe



(a)

Image of Class Pred Probability – Fe



(b)

**FIGURE 15:**  $\mu$ XRF map of iron (Fe) element following the classical analytical approach (a) and the PLS-DA prediction modelling (b).

shows a correct identification in the electronic component characterized by a high lead presence. Its recognition is difficult in all those components of smaller dimensions, probably for the presence of other elements (i.e. Bismuth (La 10.839 KeV) whose peaks produce a masking effect (i.e. Pb La 10.551 KeV). (Figure 14b).

The map of iron (Fe) shows a high concentration of this element on card and security holders (Figure 15a). The prediction map, as resulting from PLS-DA modelling, produces its correct identification (Figure 15b).

#### 4. CONCLUSIONS

The study was carried out to investigate the utilization of chemometric procedures, based on processing of data set generated by  $\mu$ XRF, in order to perform a laboratory scale preliminary (i.e. before mechanical-physical processing) automatic check of end-of-life (EOL) iPhone electronic boards characteristics (i.e. manufacturing and components presence), and related recovered products (i.e. particles) derived from processing. More in detail, PLS-DA, after PCA, was applied to build a model able to recognize/classify the precious and rare earth elements starting from the reference energy spectra representative of the different elements object of investigations.

The proposed combined chemometric- $\mu$ XRF approach presents a lot of advantages: it is objective, it does not require any preliminary knowledge of the sample and it allows to assess, in a relative simple way, the quantity of precious and rare earth elements that is possible to extract by PCB derived products (i.e. iPhone electronic boards and products resulting from their mechanical processing).

The proposed prediction model performs a good classification. The procedure, after the preliminary model recognition set up, is easy to implement and it is characterized by low operative costs, being the procedure totally software, especially if compared with classical methods usually requiring sample chemical pre-treatment and longer analytical time (i.e. ICP-OES and SEM-EDX).

Further studies will be addressed to a systematic application of the proposed approach to particle resulting from comminution, classification and physical separation of dismissed iPhone boards, and more in general, PCB, in order to perform not only a qualitative control of the different flow streams, but also to set up pre-concentration actions finalized to separate particles characterized by different precious and rare earth elements composition and distribution. Following this approach, it will be thus possible to design more efficient and specialized strategies for final elements recovery by chemical processing.

#### REFERENCES

Ballabio D. and Consonni V. (2013). Classification tools in chemistry. Part 1: linear models. PLS-DA. *Analytical Methods*, 5(16), 3790-3798.

- Bonifazi G., Serranti S., Potenza F., Luciani V. and Di Maio F. (2017) Gravity packaging final waste recovery based on gravity separation and chemical imaging control. *Waste Management*, 60, 50-55.
- Bro R. and Smilde A. K. (2014). Principal component analysis. *Analytical Methods*, 6(9), 2812-2831.
- Carvalho R.R.V, Coelho J.A.O, Santos J.M., Aquino F.W.B., Carneiro R.L., Pereira-Filho E.R. (2015). Laser-induced breakdown spectroscopy (LIBS) combined with hyperspectral imaging for the evaluation of printed circuit board composition. *134(1)*, 278-283.
- Chakhmouradian A. R. and Wall F. (2012). Rare earth elements: minerals, mines, magnets (and more). *Elements*, 8(5), 333-340.
- European Commission, (2008). COM 699 - The raw materials initiative—meeting our critical needs for growths and jobs in Europe. Brussels, SEC (2008), 2741.
- De Vito I. E., Olsina R. A. and Masi A. N. (2000). Enrichment method for trace amounts of rare earth elements using chemofiltration and XRF determination. *Fresenius' journal of analytical chemistry*, 368(4), 392-396.
- European Commission, 2010. Critical Raw Material for the EU – Report of the Ad-hoc Working Group on Defining Critical Raw Materials. European Commission (EC).
- Figuerola R. G., Lozano E., Belmar F., Alcaman D., Bohlen A., Oliveira C. A. B., Silva A.L.M. and Veloso J.F.C.A. (2014). Characteristics of a robust and portable large area X-ray fluorescence imaging system. *X-Ray Spectrometry*, 43(2), 126-130.
- Gallardo, H., Queralt, I., Tapias, J., Guerra, M., Carvalho, M. L. and Marguí, E. (2016). Possibilities of low-power X-ray fluorescence spectrometry methods for rapid multielemental analysis and imaging of vegetal foodstuffs. *Journal of Food Composition and Analysis*, 50, 1-9.
- Guerra, M. B. B., Schaefer, C. E., de Carvalho, G. G., de Souza, P. F., Júnior, D. S., Nunes, L. C. and Krug, F. J. (2013). Evaluation of micro-energy dispersive X-ray fluorescence spectrometry for the analysis of plant materials. *Journal of Analytical Atomic Spectrometry*, 28(7), 1096-1101.
- Hagelüken C. and Corti C. W. (2010). Recycling of gold from electronics: Cost-effective use through 'Design for Recycling'. *Gold Bulletin*, 43(3), 209-220.
- Kumar K., Saion E., Halimah M. K., Yap C. K. and Hamzah M. S. (2014). Rare earth element (REE) in surface mangrove sediment by instrumental neutron activation analysis. *Journal of Radioanalytical and Nuclear Chemistry*, 301(3), 667-676.
- Massari S. and Ruberti M. (2013). Rare earth elements as critical raw materials: Focus on international markets and future strategies. *Resources Policy*, 38(1), 36-43.
- Nikonow, W. and Rammlmair, D. (2016). Risk and benefit of diffraction in Energy Dispersive X-ray fluorescence mapping. *Spectrochimica Acta Part B: Atomic Spectroscopy*, 125, 120-126.
- Palmieri R., Bonifazi G. and Serranti S. (2014) Recycling-oriented characterization of plastic frames and printed circuit boards from mobile phones by electronic and chemical imaging. *Waste Management*, 34(11), 2120-2130.
- Smoliński, A., Stempin, M. and Howaniec, N. (2016). Determination of rare earth elements in combustion ashes from selected Polish coal mines by wavelength dispersive X-ray fluorescence spectrometry. *Spectrochimica Acta Part B: Atomic Spectroscopy*, 116, 63-74.
- Tiess G. (2010). Minerals policy in Europe: Some recent developments. *Resources Policy*, 35(3), 190-198.
- Zawisza A., Pytlakowska K., Feist B., Polowniak M. and Kita A. (2011). Determination of rare earth elements by spectroscopic techniques: a review. *J. Anal. Atom. Spectrom.*, 26 (12), 2373–2390.
- Zhang Y., Jiang, Z., He M. and Hu (B. 2007). Determination of trace rare earth elements in coal fly ash and atmospheric particulates by electrothermal vaporization inductively coupled plasma mass spectrometry with slurry sampling. *Environ. Pollut.*, 148 (2), 459–467
- Zhou Y. and Qiu K. (2010). A new technology for recycling materials from waste printed circuit boards. *Journal of Hazardous Materials*, 175(1), 823-828.